Chiral *p*-wave superconductivity in $Pb_{1-x}Sn_xTe$: Signatures from bound-state spectra and wave functions

S. Kundu* and V. Tripathi

Department of Theoretical Physics, Tata Institute of Fundamental Research, Homi Bhabha Road, Navy Nagar, Colaba, Mumbai 400005

(Received 26 October 2018; published 6 May 2019)

Surface superconductivity has recently been observed on the (001) surface of the topological crystalline insulator $Pb_{1-x}Sn_xTe$ using point-contact spectroscopy and theoretically proposed to be of the chiral *p*-wave type. In this paper, we closely examine the conditions for realizing a robust chiral *p*-wave order in this system rather than conventional *s*-wave superconductivity. Further, within the *p*-wave superconducting phase, we identify parameter regimes where impurity bound (Shiba) states depend crucially on the existence of the chiral *p*-wave order and distinguish them from other regimes where the chiral *p*-wave order does exist but the impurity-induced subgap bound states cannot be used as evidence for it. Such a distinction can provide an easily realizable experimental test for chiral *p*-wave order in this system. As a possible application of our findings, we also show that the zero-energy Shiba states in point defects possess an internal SU(2) rotational symmetry which enables them to be useful as quantum qubits.

DOI: 10.1103/PhysRevB.99.205105

I. INTRODUCTION

Topological superconductors [1–3] have received considerable attention in recent times, motivated by the desire to realize Majorana fermions in material systems [4–10]. While there has been a tremendous effort toward engineering topological superconductivity by means of an induced *p*-wave pairing, through, for instance, the proximity effect in topological insulators [4,6] or hybrid structures of semiconductors and superconductors [5,7,8] intrinsic topological superconductors are still quite rare, with Sr_2RuO_4 [11–13] and $Cu_xBi_2Se_3$ [14–16] being popular candidates for realizing such a state. There is considerable current interest in topological insulator surfaces as an environment where two-dimensional topological superconductivity can be realized, which is protected against weak disorder by *s*-wave Cooper pairing in the bulk [17]. This makes the superconductivity much more robust than in, say, Sr_2RuO_4. Recently, we showed [18,19], using a parquet renormalization group analysis [20], that in the presence of weak correlations, the electronic ground state on the (001) surface of the topological crystalline insulator (TCI) $Pb_{1-x}Sn_xTe$ [21–27] corresponds to a chiral *p*-wave superconducting state. Low-lying Type-II Van Hove singularities [28], peculiar to the (001) surface of this material, serve to enhance the transition temperature to values parametrically higher than those predicted by BCS theory [29]. Since the surface electronic bands are effectively spinless, *s*-wave superconductivity is precluded, unless pairing occurs between electrons in different time-reversed bands, which is ruled out at sufficiently low carrier densities. Here the nontrivial Berry phases associated with the electronic wave functions ultimately dictate the chiral *p*-wave symmetry of the superconducting order parameter. $Pb_{1-x}Sn_xTe$ thus provides a good meeting ground for various desirable attributes, under extremely accessible conditions, which is not commonly encountered.

On the experimental front, recent point-contact spectroscopy measurements have confirmed the existence of superconductivity of the (001) surface of this system, but the nature of the superconducting order is yet to be ascertained. The superconductivity is indicated by a sharp fall in the resistance of the point contact below a characteristic temperature (3.7–6.5 K) [30] and the appearance of a spectral gap with coherence peaklike features and zero-bias anomalies [30,31]. However, contrary to the claim in Ref. [31], these zero-bias peaks are not necessarily signatures of Majorana bound states. Indeed, such features may appear in point-contact spectroscopy measurements whenever the tunnel junction is not in the ballistic regime [32]. Similarly, zero-bias anomalies appearing in scanning tunneling spectra have been discussed extensively as signatures of Majorana bound states [4–6,8] but may often originate from other independent causes such as band-structure effects [33] and stacking faults [34]. Moreover, while it has been shown that Majorana bound states can indeed be realized at the end points of linear defects in a chiral *p*-wave superconductor [35], these may not exist for other types of surface defects, such as pointlike ones, or may be difficult to detect. An alternate strategy would be to go beyond the Majorana states and instead look for Shiba-like states [36–38] for probing the superconducting order [39–46]. However, in $Pb_{1-x}Sn_xTe$, given the sensitivity of the underlying order to small changes in parameters such as doping and time-reversal symmetry breaking fields, it is necessary to examine under what circumstances Shiba-like states can form and can be used to unambiguously establish topological superconductivity in this system.

In this paper, we identify the parameter regimes where superconductivity may exist on the (001) surface of $Pb_{1-x}Sn_xTe$ and show that for small changes in doping, the nature of the superconducting order can change from a topological chiral *p*-wave type to a conventional *s*-wave type. Shiba-like subgap states do not exist for potential defects in *s*-wave

*Corresponding author: sarbajaya@theory.tifr.res.in

superconductors. On the other hand, in the chiral p-wave superconducting state, we find two distinct parameter regimes, only one of which can be used to reliably establish the existence of chiral p-wave superconductivity using impurity-induced Shiba-like states. In our treatment, we obtain exact analytical expressions for the bound-state spectra and wave functions, as a function of the parameters of the system, which shed light on several notable characteristics of these bound states. We show that the azimuthal angle-dependence of the wave functions in point defects can be used to distinguish between nodal and chiral superconductors. We have obtained exact analytical expressions for the bound-state wave function in a point defect, which qualitatively agree with Ref. [44], with differences related to the localization length. Incidentally, other approximate solutions proposed in the literature based on different variational ansatzes [39,47] are inconsistent with our exact solutions. For the case of point defects, we find that the wave function corresponding to the zero-energy bound state has an internal SU(2) rotational symmetry which makes it useful as a quantum qubit. If chiral p-wave superconductivity is indeed established on the surface of $Pb_{1-x}Sn_xTe$, then such qubits would be relatively easy to realize and manipulate using, say, STM tips [48]. The above properties, together with the constraints that we impose on the parameter regimes, can help identify the nature of the surface superconducting order in $Pb_{1-x}Sn_xTe$.

The rest of the paper is organized as follows. In Sec. II, we describe the surface band structure in the vicinity of the $\overline{X}$ points on the (001) surface in the presence of a time-reversal symmetry breaking perturbation, discuss the various parameter regimes for the existence and nature of the surface superconductivity, and introduce the Bogoliubov–de Gennes (BdG) Hamiltonian that is considered in the rest of the analysis. In Sec. III, we discuss impurity-induced bound states in doped semiconductors and the existence of subgap bound states in certain parameter regimes, both in the presence and absence of chiral p-wave order. In Sec. IV, we derive the general condition for realizing subgap bound states trapped in isolated potential defects in a chiral p-wave superconductor, obtain analytical expressions for the bound-state spectra and wave functions and show that no such in-gap states are possible in the presence of s-wave superconductivity. In Sec. V, we derive the corresponding expressions for the specific case of $Pb_{1-x}Sn_xTe$, for both point and linear defects, when the chemical potential is either tuned within the gap created by the Zeeman field or intersects the lower surface conduction band. Finally, in Sec. VI, we discuss the primary imports of our work, possible issues related to its practical realization, and future directions.

II. SURFACE BAND STRUCTURE AND ELECTRONIC INSTABILITIES

The band-gap minima of IV-VI semiconductors are located at the four equivalent L points in the FCC Brillouin zone. In Ref. [24], these are classified into two types: *Type-I*, for which all four L points are projected to the different time-reversal invariant momenta in the surface Brillouin zone, and *Type-II*, for which pairs of L points are projected to the same surface momentum. The (001) surface belongs to the latter class of surfaces, for which the L_1 and L_2 points are projected to the $\overline{X_1}$ point on the surface, and the L_3 and L_4 points are projected to the symmetry-related $\overline{X_2}$ point. This leads to two coexisting massless Dirac fermions at $\overline{X_1}$ arising from the L_1 and the L_2 valley, respectively, and likewise at $\overline{X_2}$. The $k.p$ Hamiltonian close to the point $\overline{X_1}$ on the (001) surface is derived on the basis of a symmetry analysis in Ref. [24] and is given by

$$H_{\overline{X_1}}(k) = (v_x k_x s_y - v_y k_y s_x) + m\tau_x + \delta s_x \tau_y, \tag{1}$$

where k is measured with respect to $\overline{X_1}$, $\vec{s}$ is a set of Pauli matrices associated with the two $j = \frac{1}{2}$ angular momentum components for each valley, τ operates in valley space, and the terms m and δ account for single-particle intervalley scattering processes. In our analysis, we shall focus entirely on the surface band structure in the vicinity of these two inequivalent points, which are henceforth referred to as $\overline{X}$. The surface Hamiltonian corresponding to each of the $\overline{X}$ points consists of four essentially spinless bands. The two bands lying closest to the chemical potential of the parent material each feature two Dirac points at $(0, \pm\sqrt{m^2+\delta^2}/v_y)$ as well as two Van Hove singularities at $(\pm m/v_x, 0)$, while the bands lying farther away in energy have a single Dirac-cone structure. The two positive energy bands (and likewise the two negative energy ones) touch each other at the $\overline{X}$ point (due to time-reversal symmetry), with a massless Dirac-like dispersion in its vicinity. We introduce a Zeeman spin-splitting term Ms_z in the noninteracting surface Hamiltonian [19] in Eq. (1), which lifts the degeneracy between the two bands at the $\overline{X}$ point and results in the following dispersions for the four surface bands:

$$\epsilon_{k,\pm} = \pm\sqrt{k_x^2 v_x^2 + k_y^2 v_y^2 + m^2 + \delta^2 + M^2 \pm 2\sqrt{M^2 m^2 + k_x^2 m^2 v_x^2 + k_y^2 (m^2+\delta^2) v_y^2}}. \tag{2}$$

For surface momenta (k_x, k_y) in the vicinity of the $\overline{X}$ point, we now have a massive Dirac-like dispersion, which can be approximately written as

$$\epsilon_{k_x,k_y} = C - A\left(k_x^2 + k_y^2\right), \tag{3}$$

for the lower energy surface band, with $C = \sqrt{(M-m)^2+\delta^2}$ and $A \sim 1/(MC)$, measured with respect to the pair of Dirac points lying on either side of the $\overline{X}$ point. Since we are interested in low values of doping, we will confine our attention the regime corresponding to small momenta (k_x, k_y), where $M < m$. Figure 1 shows the surface band structure in the vicinity of the $\overline{X}$ point for various values of the spin-splitting M.

Electron correlations can lead to electronic instabilities of various kinds on the (001) surface of $Pb_{1-x}Sn_xTe$. Since the Fermi surface is approximately nested, Fermi surface instabilities of both particle-particle and particle-hole type can occur in the lower surface conduction band. In Refs. [18] and [19], we studied electronic phase competition for electrons in

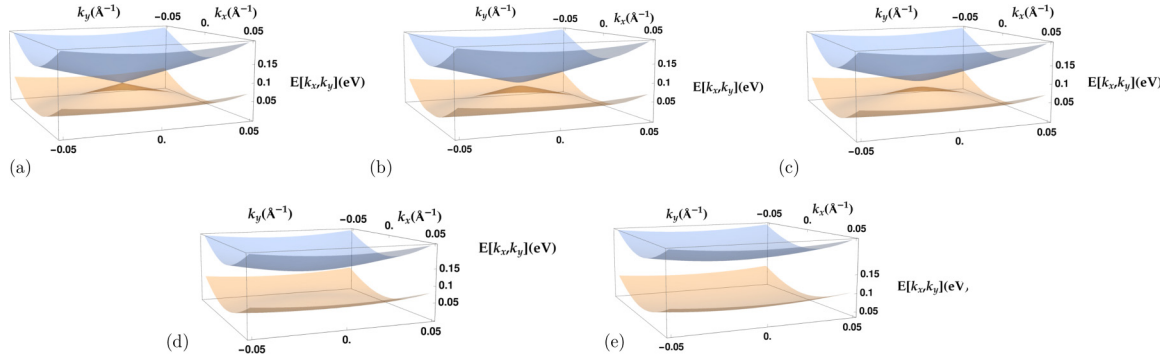

FIG. 1. The band structure of the two upper surface bands in the vicinity of the $\overline{X}$ point as a function of (k_x, k_y) in the presence of a Zeeman spin-splitting of magnitude M of different strengths; (a) $M = 0.0$, (b) $M = 0.005$, (c) $M = 0.01$, (d) $M = 0.05$, and (e) $M = 0.1$ (in eV). Note that a gap is introduced at the $\overline{X}$ point as M is turned on, and with increasing values of M, this gap increases, and the curvature of the lower band gradually changes sign. A change in the curvature can also affect the nature of the impurity-induced bound states realized in the chiral p-wave superconducting state. In the paper, we work in the regime $M < m$, where the mass term $m = 0.07$ eV determines the value of the energy at the $\overline{X}$ point measured with respect to the pair of Dirac points.

this band by treating both these types of channels on an equal footing. In almost all situations where an instability occurs, we found that chiral p-wave superconductivity is favored as long as interband scattering is neglected.

In our analysis of impurity-induced bound states in the chiral p-wave superconducting state, we will work with the following BdG Hamiltonian:

$$H_0(k) = \begin{bmatrix} \epsilon_{k_x,k_y} - \mu & \Delta(k_x - ik_y) \\ \Delta(k_x + ik_y) & -\epsilon_{k_x,k_y} + \mu \end{bmatrix}, \tag{4}$$

where ϵ_{k_x,k_y} refers to the noninteracting dispersion in Eq. (3) and μ refers to the chemical potential. This Hamiltonian acts in the Nambu space $(c_k, c^\dagger_{-k})$, where c_k are the effectively spinless fermions in the lower-energy surface band and $\Delta_k \equiv < c_k c_{-k} > = \Delta(k_x - ik_y)$ is the superconducting order parameter. In the absence of Δ, Eq. (4) would correspond to two copies of the Hamiltonian of a nonrelativistic particle whose energies are reckoned from an arbitrary value μ. This situation is explained in more detail in Sec. III below.

Substituting the expression for $\epsilon_{k_x k_y}$ from Eq. (3) above, the spectrum corresponding to the Nambu Hamiltonian in Eq. (4) is given by $E = \pm\sqrt{(Ak^2 + \mu')^2 + \Delta^2 k^2}$, where $k^2 = k_x^2 + k_y^2$ and $\mu' = \mu - C$ is an effective chemical potential reckoned from the top of the band, corresponding to the energy value closest to the higher energy surface band. We introduce dimensionless quantities

$$\lambda = \frac{\Delta^2}{2A|\mu'|} \tag{5}$$

and

$$\epsilon = \frac{E}{|\mu'|}, \tag{6}$$

which appear frequently in the rest of our analysis. For nonzero values of μ, the spectrum of the BdG Hamiltonian is gapped if Δ is finite. We look specifically for bound states which lie within the gap.

In general, the nature of surface electronic instabilities, and their consequences for impurity-induced bound states, depend crucially on the position of the chemical potential with respect to the surface bands. A schematic of the band structure around the $\overline{X}$ point on the (001) surface, together with various representative positions for the chemical potential is shown in Fig. 2. If the gap is sufficiently large and the Fermi level does not intersect the upper band, then (interband) s-wave superconductivity, which occurs in case (a) of Fig. 2, is precluded. In the rest of the paper, we shall work in this regime. For the case (b) in Fig. 2 where the chemical potential does not intersect the lower surface conduction band, the band gap is conventional, as in, say, a semiconductor, and we

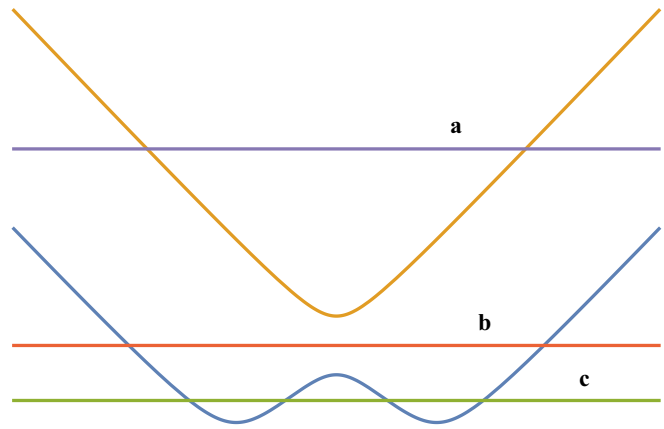

FIG. 2. Schematic illustration of the band structure in the vicinity of the $\overline{X}$ point, and three different doping regimes that can either result in qualitatively different electronic instabilities on the (001) surface of $Pb_{1-x}Sn_xTe$ (i.e., either conventional s-wave or chiral p-wave order) or lead to a difference in the nature of impurity-induced bound states realized in a chiral p-wave superconducting state. In (a), the Fermi level intersects two of the surface bands, which are time-reversed counterparts. In this case, interband pairing of electrons gives rise to s-wave superconductivity, and no Shiba-like states exist for potential defects on the surface. In (b) and (c), the pairing of the surface electrons is of the chiral p-wave type. We show in the paper that only the latter case, (c), when the Fermi level intersects the lower surface conduction band, Shiba-like subgap states can be unambiguously attributed to the presence of topological superconductivity.

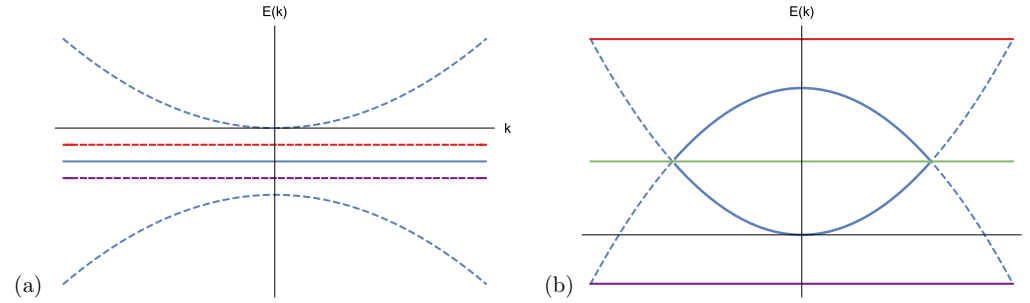

FIG. 3. Schematic illustration of the Nambu bands when (a) $\mu < 0$, and the chemical potential lies in the gap (b) $\mu > 0$ and the chemical potential intersects the bands, in the absence of the chiral p-wave order parameter Δ. The bound-state energies denoted by the red and purple lines lie within the gap in (a) and intersect the bands in (b). The chemical potential μ lies in the center and is denoted by the blue line in (a) and the green line in (b). The filled and empty part of the bands are represented by solid and dashed lines, respectively. Clearly, in (a) both the bands as well as the impurity states are empty.

call it *normal*. For the case (c) in Fig. 2, where it intersects this band, an additional band gap opens up at the points of intersection (not depicted in Fig. 2), due to the presence of the chiral p-wave superconducting order. This corresponds to an *inverted* band gap.

In the next section, we will try to understand the origin of impurity-induced states in the regimes (b) and (c) and how they differ from each other in the presence and absence of a chiral p-wave order. The role played by the distinction between these regimes in identifying the chiral p-wave nature of the superconducting order forms a crucial part of our paper.

III. IMPURITY STATES IN DOPED SEMICONDUCTORS

It is well known that in one dimension, a bound state always exists for a nonrelativistic particle in the presence of an attractive Delta-function potential. Consider a single impurity in a semiconductor, and writing down the Schrodinger equation in momentum space, we have

$$(\epsilon_k - \mu)\psi_k + \int dk' V_{k,k'}\psi_{k'} = E\psi_k, \tag{7}$$

where $V_{k,k'} = V_0$ and μ denotes the chemical potential. Using

$$\psi_k = \frac{-V_0 \int dk' \psi_{k'}}{(\epsilon_k - \mu - E)}$$

and integrating both sides over the momentum k, we obtain the following condition on the defect potential strength V_0 for realizing impurity-induced bound states:

$$V_0 = \frac{-1}{\int \frac{dk}{(\epsilon_k - \mu - E)}},$$

which always gives rise to a solution, provided the integrand does not have any real poles. When such impurity bound states are present, they appear at an energy value proportional to $\sqrt{V_0}$ below the bottom of the conduction band and move further downward as V_0 increases. If ϵ_k is the valence band of a semiconductor, then the V_0 must be positive, and the bound states appear above the top of the valence band. The existence of the impurity band is independent of the chemical potential μ, but the chemical potential determines whether the impurity band is occupied or not.

Now the same problem can be reexpressed in the Nambu representation by introducing another copy of the problem which is related to the first one by a particle-hole transformation. In the Nambu representation, the impurity bound states appear exactly as discussed above, except that since there are now two copies, for each positive impurity level, there is a corresponding negative one with the same magnitude. Consider the example of an impurity bound state arising from donor dopants in a semiconductor, and $\epsilon_k > 0$ corresponds to the conduction band. The chemical potential is the reference energy from which all energies are measured, and in this case, the negative value of μ implies that the chemical potential does not intersect the bands, and both the bands are empty. This is illustrated in Fig. 3(a) above. On the other hand, when $\mu > 0$, the bands as well as the impurity levels cross the Fermi level and become occupied, resulting in a new situation depicted in Fig. 3(b). This is merely an artifact of the chemical potential changing sign and the levels that have crossed are those whose nature has changed from being empty to being occupied.

The situation changes dramatically in the presence of a chiral p-wave superconducting order. If the chemical potential $\mu < 0$, then the impurity levels remain empty but the bands shift in magnitude, as shown in Fig. 4(a). Here we continue to obtain subgap states and the impurity levels are indistinguishable from those in semiconductors. However, when $\mu > 0$, the presence of superconductivity introduces a gap at the points where the two dispersing bands intersected, as shown in the Fig. 4(b). In this regime, the impurity levels which were formerly present only near the extrema of the upper and lower Nambu bands abruptly collapse to take values within the gap, and therefore we now obtain subgap states.

Thus, in the presence of a chiral p-wave order, if $\mu < 0$, then one continues to obtain subgap states which are indistinguishable from impurity states in semiconductors, while if $\mu > 0$, then new subgap states appear due to the superconducting order in the system. In the rest of the paper, we refer to the former regime of parameters as the *normal gap* regime and the latter as the *inverted gap* regime.

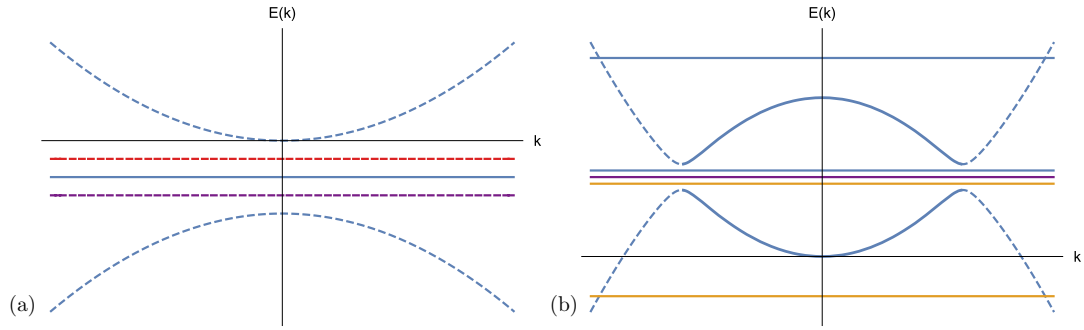

FIG. 4. Schematic illustration of the Nambu bands when (a) $\mu < 0$, and the chemical potential lies in the gap (b) $\mu > 0$ and the chemical potential intersects the bands, in the presence of the chiral p-wave order parameter Δ. Clearly, an additional band gap opens in (b) due to the superconducting order. The impurity levels denoted by the red and purple lines in (a) lie within the gap, while in (b), a pair of impurity levels denoted by blue and yellow lines lie within the smaller gap while another pair intersects the two bands. The chemical potential μ lies in the center and is denoted by the blue line in (a) and the purple line in (b). The filled and empty part of the bands are represented by solid and dashed lines respectively. In (a), both the bands as well as the impurity states are empty. These cases are discussed in detail in Secs. IV and V.

IV. CONDITIONS FOR SUBGAP BOUND STATES WITH δ-POTENTIAL DEFECTS

We now derive the general condition for realizing subgap bound states localized in one or more directions, associated with point or linear defects on the surface of the TCI. We model such defects by a multidimensional Dirac delta function $V(x_i) = V_0 \prod_i \delta(x_i)$, where i refers to the dimension, and V_0 represents the strength of the defect potential. The delta-function approximation for the potential defects is justified, provided that the defect potential is sufficiently smooth on the scale of the lattice constant (to avoid scattering processes between the $\overline{X_1}$ and $\overline{X_2}$ points) but, nevertheless, short-ranged compared to the wavelength of the electrons.

The Schrödinger equation in momentum space, in the presence of the defect potential, is given by

$$H_0(k)\psi_k + \int (d^d k')V_{k,k'}\psi_{k'} = E\psi_k, \tag{8}$$

where $H_0(k)$ is defined in Eq. (4) above, E refers to the value of the bound-state energy, and $V_{k,k'} = V_0\sigma_z$ for the case of a point defect and $2\pi V_0\delta(k_y - k_y')\sigma_z$ for a linear defect along the y direction. In the latter case, the integration over k_y' gets rid of the Delta function, leading to an equation which is diagonal in k_y but mixes the k_x components.

Inverting Eq. (8), we have

$$\psi_k = -[H_0(k) - EI]^{-1}V_0\sigma_z \int (d^d k')\psi_{k'}, \tag{9}$$

where it is understood in Eq. (9) above and also in the analysis that follows that the integration runs only over k_x for a linear defect along the y direction. Next, we integrate both sides over k, cancel the common term $\int (d^d k)\psi_k$ on both sides, and arrive at the following condition:

$$\mathrm{Det}\left\{ -\int (d^d k)[H_0(k) - EI]^{-1}V_0\sigma_z - I \right\} = 0, \tag{10}$$

for the bound state. Here the integration over each component of k ranges from $-\infty$ to ∞. Note that when $\int (d^d k)\psi_k = 0$, the wave function vanishes at the origin, and the above condition is no longer applicable, since we cannot cancel the common terms. This is, for example, true for topologically nontrivial zero-energy Majorana bound states in linear defects, for which the real-space wave function acquires its peak values at the physical ends of the defect and decays into the interior. When the defect being considered is infinitely long in one of the directions, the ends not being a part of the system, one cannot mathematically realize Majorana bound states within this approach. Here we have explicitly excluded such states from consideration.

Using the expression for $H_0(k)$ in Eq. (4), the condition in Eq. (10) translates to

$$\mathrm{Det}\begin{bmatrix} -V_0 I_1(0,0,E) - 1 & V_0 I_3(0,0,E) \\ -V_0 I_4(0,0,E) & -V_0 I_2(0,0,E) - 1 \end{bmatrix} = 0, \tag{11}$$

where we define

$$I_{1,2}(x,y,E) = \int_{-\infty}^{\infty} (dk_x)(dk_y)\exp[ik_x x]\exp[ik_y y] \times \frac{\epsilon_{k_x,k_y} - \mu \pm E}{\left(\epsilon_{k_x,k_y} - \mu\right)^2 - E^2 + \Delta^2\left(k_x^2 + k_y^2\right)}, \tag{12}$$

and

$$I_{3,4}(x,y,E) = \int_{-\infty}^{\infty} (dk_x)(dk_y)\exp[ik_x x]\exp[ik_y y] \times \frac{\Delta(k_x \mp ik_y)}{\left(\epsilon_{k_x,k_y} - \mu\right)^2 - E^2 + \Delta^2\left(k_x^2 + k_y^2\right)}. \tag{13}$$

Let us consider first the case of point defects. From Eq. (11), we obtain the following condition for the strength of the defect potential V_0 that gives a bound state at energy E:

$$[V_0 I_1(0,0,E) + 1)(V_0 I_2(0,0,E) + 1] = 0. \tag{14}$$

From Eq. (14), it is evident that for a given value of V_0, we have a pair of bound states with energies $\pm E$, which is a reflection of particle-hole symmetry of the BdG Hamiltonian. Conversely, for every value of the bound-state energy there exist two possible values for the strength of the defect potential, V_0, which do not in general have the same magnitude, for which one may realize such a state.

For a line defect of infinite length along, say, the y direction, the defect potential may be written as $V(x) = V_0\delta(x)$,

such that the translational symmetry is broken only along the x direction. In this case, we obtain, from Eq. (11), the following condition for realizing a subgap bound state with an energy E, where k_y is conserved and takes real values,

$$[V_0 I_1(0,0,E)+1][V_0 I_2(0,0,E)+1] + V_0^2 I_3(0,0,E) I_4(0,0,E) = 0. \tag{15}$$

The relation between V_0 and E is

$$V_0(E) = \frac{-(I_1+I_2) \pm \sqrt{(I_1-I_2)^2 - 4I_3 I_4}}{2(I_1 I_2 + I_3 I_4)}. \tag{16}$$

Since V_0 is real, the discriminant must be positive, resulting in a condition which relates the allowed values of the bound-state energy to the quantum number k_y, i.e., $\min[E_g^2, (\mu')^2] \geqslant E^2 \geqslant \Delta^2 k_y^2$. The lowest-energy bound states clearly correspond to the case where $k_y = 0$. This leads to the conditions $1 + I_1 V_0 = 0$ or $1 + I_2 V_0 = 0$.

From Eq. (9), we can also obtain expressions for the bound-state wave functions. Taking an inverse Fourier transform on both sides, we obtain the following expression for the wave function in real space:

$$\psi(x,y) = \begin{bmatrix} a(x,y) \\ b(x,y) \end{bmatrix} = (-V_0) \begin{bmatrix} I_1(x,y,E) a_0 - I_3(x,y,E) b_0 \\ I_2(x,y,E) b_0 + I_4(x,y,E) a_0 \end{bmatrix}, \tag{17}$$

where $\psi_0 = \binom{a_0}{b_0}$ is the real-space wave function at the origin, i.e., $\psi(0,0)$, and $I_{1,2}(x,y,E)$ and $I_{3,4}(x,y,E)$ are as defined in Eqs. (12) and (13). The normalization condition is

$$\int dx \int dy [|a(x,y)|^2 + |b(x,y)|^2] = 1. \tag{18}$$

For the case of a point defect, we find that, for any nonzero value of the bound-state energy E, putting $x = y = 0$ on both sides of Eq. (17) above results in the elimination of one of the components a_0 or b_0 when the condition in Eq. (14) is satisfied. For $E = 0$, however, it simply gives rise to a consistency condition without yielding any new information about the components at the origin, and the only constraint on the constants a_0 and b_0 is then the normalization condition in Eq. (18). This is a manifestation of an internal SU(2) rotational symmetry (in particle-hole space), which makes the zero-energy state centered at the origin useful as a possible quantum qubit. A similar condition is also obtained for a linear defect, but in the specific case where $k_y = 0$. Since there are arbitrarily close bound states parametrized by nonzero k_y, the zero-energy state is not useful as a qubit for the case of linear defects.

A. Absence of subgap states for s-wave superconductivity

As discussed in Sec. II, pairing between time-reversed surface bands can lead to s-wave superconductivity on the (001) surface. We shall now show that subgap bound states in isolated potential defects can no longer be realized for a conventional s-wave superconducting order in this system.

The s-wave order parameter can be written as Δ, which is a momentum-independent constant. Following Eq. (11), the condition for realizing subgap bound states with an energy E in the presence of surface potential defects in this case is given by

$$\mathrm{Det} \begin{bmatrix} -V_0 \int (dk_x)(dk_y) \frac{\epsilon_{k_x,k_y} - \mu + E}{(\epsilon_{k_x,k_y} - \mu)^2 - E^2 + \Delta^2} - 1 & V_0 \int (dk_x)(dk_y) \frac{\Delta}{(\epsilon_{k_x,k_y} - \mu)^2 - E^2 + \Delta^2} \\ -V_0 \int (dk_x)(dk_y) \frac{\Delta}{(\epsilon_{k_x,k_y} - \mu)^2 - E^2 + \Delta^2} & -V_0 \int (dk_x)(dk_y) \frac{\epsilon_{k_x,k_y} - \mu - E}{(\epsilon_{k_x,k_y} - \mu)^2 - E^2 + \Delta^2} - 1 \end{bmatrix} = 0. \tag{19}$$

From Eq. (19), the possible values of $V_0(E)$ are given by

$$V_0 = \frac{-(a+b) \pm \sqrt{(a-b)^2 - 4c^2}}{2(ab + c^2)},$$

where $a, b = \int (dk_x)(dk_y)(\epsilon_{k_x,k_y} - \mu \pm E)/[(\epsilon_{k_x,k_y} - \mu)^2 - E^2 + \Delta^2]$ and $c = \int (dk_x)(dk_y)\{\Delta/[(\epsilon_{k_x,k_y} - \mu)^2 - E^2 + \Delta^2]\}$. Clearly, real values of V_0 require the discriminant to be positive, i.e., $|E| \geqslant \Delta$, and thus no subgap bound states are possible. The above arguments also hold true for a mixed $s + p$–wave superconducting order.

V. BOUND-STATE SPECTRA AND WAVE FUNCTIONS

We now use the results obtained in Sec. IV above in the context of subgap impurity bound states in $Pb_{1-x}Sn_xTe$. In the analysis that follows, we shall distinguish between the situations where the chemical potential lies within the conventional or *normal* band gap between the pair of surface bands and those where it intersects the lower surface conduction band, giving rise to an *inverted* band gap at small momenta. We shall find that the subgap states that arise in the *inverted band gap* situation crucially depend on the existence of the chiral p-wave order. On the other hand, in the *normal band gap* situation, the impurity bound states are not qualitatively affected in the limit where the chiral p-wave order is absent. Note that in what follows, we will be working with the valence band, as that is the physical situation prevailing in our system, and without loss of generality, the considerations discussed in Sec. III are carried through.

A. Point defects

Let us first consider the case of a point defect. In plane polar coordinates, Eq. (14), relating the impurity strength to the bound-state energy E, takes the form

$$\frac{1}{V_0} = \frac{1}{4\pi} \int_0^{\Lambda^2} d\upsilon \frac{(A\upsilon + \mu') \mp E}{(A\upsilon + \mu')^2 - E^2 + \Delta^2 \upsilon}, \tag{20}$$

where $\upsilon = k^2$ and $\mu' \equiv \mu - C$, and Λ is the large momentum cutoff, physically corresponding to the inverse of the width

of the potential well, which is approximated to be a Delta-function potential in our treatment. We now examine Eq. (20) respectively in the *normal* and *inverted* band gap regimes.

1. Conditions for bound states in different parameter regimes

(a) Normal band gap: $\mu' > 0$. When the chemical potential $\mu > C$ (or $\mu' > 0$), the condition for subgap bound states in Eq. (20) above evaluates to

$$\frac{1}{V_0} \approx \frac{1}{2A\sqrt{(\lambda+1)^2-(1-\epsilon^2)}} \times \left\{ (\lambda \pm \epsilon) \ln \left| \frac{\lambda+1-\sqrt{(\lambda+1)^2-(1-\epsilon^2)}}{\lambda+1+\sqrt{(\lambda+1)^2-(1-\epsilon^2)}} \right| + \sqrt{(\lambda+1)^2-(1-\epsilon^2)} \left[\ln \left| \frac{A^2\Lambda^4}{|\mu'|^2(1-\epsilon^2)} \right| \right] \right\}. \quad (21)$$

For any value of the bound-state energy $|E| < \mu'$, we find that $(\lambda \pm \epsilon) < \sqrt{(\lambda+1)^2-(1-\epsilon^2)}$, implying that V_0 is always a positive quantity. Physically, this corresponds to impurity (hole) states near the valence band of a semiconductor, and in this regime, one always obtains subgap states, even when Δ is turned off. The impurity levels here lie in the manner shown in Fig. 4(a).

(b) Inverted band gap: $\mu' < 0$. Here the chemical potential $\mu < C$, or $\mu' < 0$, and this corresponds to the *inverted band gap* situation, which corresponds to the expression in Eq. (21) above, with $\lambda \to -\lambda$. In this case, a gap opens either at $k = 0$ or at the points of intersection of the two Nambu bands [see Fig. 4(b)]. If, in this regime, Δ is turned off, this gap will close and the impurity levels will be pushed away to the positions originally predicted for impurity states in a semiconductor [see Fig. 3(b)].

2. Quasilocalized bound-state wave functions for point defects

Let us now calculate the expressions for the bound-state wave functions for the case of a point defect. From Eq. (17), it can be seen that the spatial dependence of the bound-state wave functions is determined by the integrals $I_{1,2}(x, y, E)$ and $I_{3,4}(x, y, E)$, defined in Eqs. (12) and (13), respectively. In plane polar coordinates, these equations assume the form

$$I_1(r) = -\frac{1}{(2\pi)^2} \int dk d\phi\, k \exp\{ikr\cos[\theta-\phi]\} \times \frac{(Ak^2+\mu') \mp E}{(Ak^2+\mu')^2 - E^2 + \Delta^2 k^2} \quad (22)$$

and

$$I_2(r,\theta) = \frac{1}{(2\pi)^2} \exp[i\theta] \int dk d\phi\, k \exp\{ikr\cos[\phi]\} \exp[i\phi] \times \frac{\Delta k}{(Ak^2+\mu')^2 - E^2 + \Delta^2 k^2}, \quad (23)$$

where $\mu' \equiv \mu - C$, $k = \sqrt{k_x^2 + k_y^2}$, and $\tan[\phi] = y/x$. We illustrate the specific case of $E = 0$ where simple analytical expressions for the wave functions can be obtained in terms of elementary functions. Qualitatively similar results are expected for other bound-state energies with $E \neq 0$. We once again consider regimes with a *normal* and an *inverted* band gap.

(a) Normal band gap: $\mu' > 0$. Using the well-known result $\int d\phi \exp\{ikr\cos[\theta-\phi]\} = 2\pi J_0(kr)$, the expression of $I_1(r)$ from Eq. (22) is as follows:

$$I_1(r) = \frac{1}{4\pi} \int dk k J_0(kr) \frac{2}{A(\alpha+\beta)} \left(\frac{\alpha}{k^2+\alpha^2} + \frac{\beta}{k^2+\beta^2} \right) = -\frac{1}{2\pi A(\alpha+\beta)} [\alpha K_0(\alpha r) + \beta K_0(\beta r)], \quad (24)$$

where $\alpha, \beta = \sqrt{\mu'/A}[(\sqrt{\lambda+2} \pm \sqrt{\lambda})/\sqrt{2}]$.

Thus, we find that $I_1(r)$ is an exponentially decaying function of at large distances r from the position of the defect. Note that when $\Delta = 0$, i.e., $\lambda = 0$, α and β are real, giving rise to exponentially decaying states.

Similarly, using the result $\int d\phi \exp\{ikr\cos[\theta-\phi]\} \exp[i\phi] = i\exp[i\theta] 2\pi J_1(kr)$, we may simplify the expression for I_2 given in Eq. (23) as

$$I_2(r,\theta) = \frac{-i\exp[i\theta]}{2\pi A(\alpha+\beta)} \int \frac{dx}{r} J_1(x) \left(\frac{x^2}{x^2+\alpha^2 r^2} - \frac{x^2}{x^2+\beta^2 r^2} \right) = \frac{-i\exp[i\theta]}{2\pi A(\alpha+\beta)} \frac{1}{r} [K_1(\alpha r) - K_1(\beta r)], \quad (25)$$

where $kr \equiv x$, $\alpha, \beta = \sqrt{\mu'/A}[(\sqrt{\lambda+2} \pm \sqrt{\lambda})/\sqrt{2}]$, and in the second line we have used the relation [49]

$$\int_0^\infty dx \frac{x J_0(ax)}{x^2+\alpha^2 r^2} = K_0(a\alpha r), \quad (26)$$

and differentiated both sides with respect to the parameter a and taken the limit $a \to 1$, to obtain Eq. (25) above. We therefore find that the function $I_2(r,\theta)$ decays exponentially at large distances.

(b) Inverted band gap: $\mu' < 0$. Here we consider a situation where $\mu < C$, or $\mu' < 0$, and repeat the analysis of the previous section by replacing μ' by $-|\mu'|$ in Eqs. (22) and (23).

For $\lambda \geqslant 2$, we then have

$$I_1(r) = \frac{1}{2\pi} \int dk\, k J_0(kr) \frac{1}{A(\alpha-\beta)} \left(\frac{2\alpha}{k^2+\alpha^2} - \frac{2\beta}{k^2+\beta^2} \right) = \frac{1}{2\pi A(\beta-\alpha)} [\alpha K_0(\alpha r) - \beta K_0(\beta r)],$$

where now $\alpha, \beta = \sqrt{\mu'/A}[(\sqrt{\lambda} \pm \sqrt{\lambda-2})/\sqrt{2}]$. Similarly, from Eq. (23), we write the expression for $I_2(r,\theta)$ as

$$I_2(r,\theta) = \frac{i}{2\pi} \exp[i\theta] \int dk\, J_1(kr) \frac{1}{(A)} \frac{1}{(\beta-\alpha)} \times \left(\frac{x^2}{x^2+\alpha^2 r^2} - \frac{x^2}{x^2+\beta^2 r^2} \right) = \frac{i\exp[i\theta]}{2\pi A(\beta-\alpha)} \frac{1}{r} [K_1(\alpha r) - K_1(\beta r)],$$

where $\alpha, \beta = \sqrt{\mu'/A}[(\sqrt{\lambda} \pm \sqrt{\lambda-2})/\sqrt{2}]$, following steps similar to the previous case, where $\mu' > 0$. The results obtained are identical for $\lambda < 2$ but with $\alpha, \beta = \sqrt{|\mu'|/A}[(\sqrt{\lambda} \mp i(\sqrt{2-\lambda}]/\sqrt{2})$. Please refer to Appendix B

for a detailed derivation of the asymptotic forms of the bound-state wave functions.

In contrast to a chiral superconductor, a nodal superconductor gives a qualitatively different wave function for the impurity bound state. For instance, when the superconducting order parameter $\Delta_k = \Delta k \cos[\phi]$, we have

$$I_2(r,\theta) = \frac{\cos[\theta]}{(2\pi)} \int dk\, k \frac{\Delta k}{(Ak^2+\mu')^2 + \Delta^2 k^2} i J_1(kr).$$

Similarly, for $\Delta_k = \Delta k \sin[\phi]$,

$$I_2(r,\theta) = \frac{\sin[\theta]}{(2\pi)} \int dk\, k \frac{\Delta k}{(Ak^2+\mu')^2 + \Delta^2 k^2} i J_1(kr).$$

Thus, unlike a chiral p-wave superconductor, the above types of superconducting order feature nodal lines in the bound-state wave function, at large distances from the position of the defect. One could use STM imaging of the bound-state wave functions as a means to distinguish between nodal and chiral p-wave order on the surface.

Incidentally, our results qualitatively differ from the bound-state wave functions proposed earlier in this context using a variational ansatz [39,47]. The asymptotic behavior of the bound-state wave functions in a point defect has also been calculated in a recent work and found to be exponentially decaying [44]. The treatment there, however, assumes a constant density of states at the Fermi surface to evaluate integrals analogous to those in Eqs. (22) and (23). This is a questionable assumption, given that the large-distance behavior is governed by small momenta, where the density of states goes to zero linearly with momentum. As a result of this approximation, the characteristic length scale over which the wave function decays has a parameter dependence that is different from ours.

B. Line defects

Here we study the nature of bound states for long linear defects. In this case, we write the defect potential as $V(x,y) = V_0\delta(x\cos[\alpha] + y\sin[\alpha])$ and consider the special case of $\alpha = 0$, i.e., $V(x) = V_0\delta(x)$. Once again, we study the two regimes with a *normal* and an *inverted* band gap, respectively.

1. Normal band gap: $\mu' > 0$

Following Eq. (15), the relation between V_0 and the bound-state energy E (for $k_y = 0$) is given by

$$\frac{1}{V_0} = \frac{1}{(2\pi)} \int_0^\infty \frac{dy}{2\sqrt{y}} \frac{(-Ay - \mu' \pm E)}{A^2(y+a)(y+b)}, \tag{27}$$

where $\mu' \equiv \mu - C$, $y = k_x^2$, and $a, b = (\mu'/A)(\lambda + 1 \mp \sqrt{[(\lambda+1)^2 - (1-\epsilon^2)]})$. Evaluating the integral in Eq. (27), we arrive at

$$V_{0,\pm} = \frac{4A(\sqrt{a}+\sqrt{b})}{[1+\sqrt{(1\mp\epsilon)/(1\pm\epsilon)}]}, \tag{28}$$

with $\sqrt{ab} = |\mu'|\sqrt{1-\epsilon^2}/A$. The variation of V_0 as a function of the bound-state energy E is shown in Fig. 5. Here we find a trivial crossing of the energy level with the chemical potential as V_0 is tuned, which does not depend on the presence of superconductivity. A similar crossing has also been observed in Ref. [41], where it has been used to characterize the topological superconducting phase. We emphasize here that the crossing that we observe is an artifact of the Nambu representation and would appear even in the absence of superconductivity. The origin of the zero-energy crossings has also been discussed in Sec. III above.

The subgap bound states in this case form a part of a continuum of states parametrized by different values of k_y. The corresponding expression obtained by solving Eq. (15) for a finite, real value of k_y is given by

$$V_{0,\pm} = \frac{2A(\sqrt{a}+\sqrt{b})\sqrt{1\pm\epsilon_e}(\sqrt{1\mp\epsilon_e}+\sqrt{1\pm\epsilon_e})}{\left(\sqrt{1-\epsilon_e^2}+1\right)},$$

with $a, b = (\mu_e/A)[\lambda_e + 1 \mp \sqrt{(\lambda_e+1)^2 - (1-\epsilon_e^2)}]$, $\mu_e = \mu' + Ak_y^2$, $E_e^2 = E^2 - \Delta^2 k_y^2$, and $\lambda_e = \Delta^2/(2A|\mu_e|)$. Clearly,

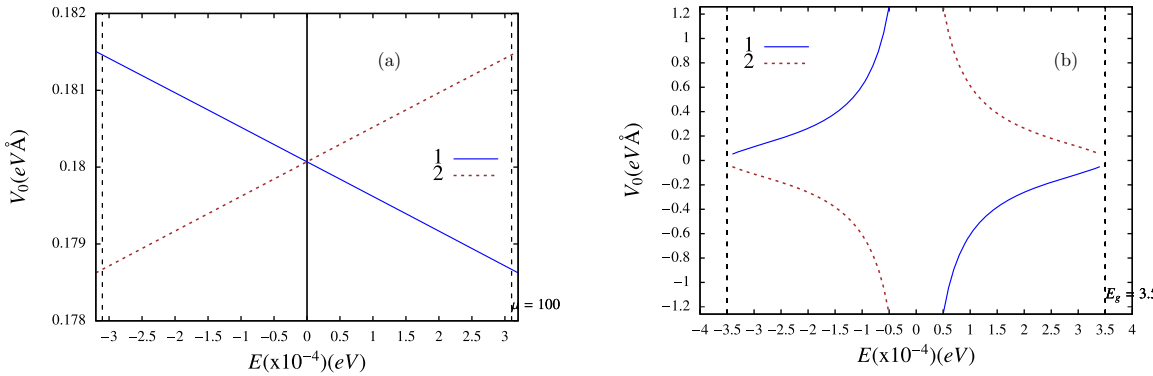

FIG. 5. The figure showing the variation in the strength of the defect potential V_0 required to give a subgap bound state as a function of the magnitude of the bound-state energy E for a line defect. The cases considered are as follows: (a) $\mu' > 0$ for a *normal* band gap and (b) $\mu' < 0$ for an *inverted* band gap. The parameters chosen are $A = 4.0$eV Å, $\mu' = 20$ meV, and $\Delta = 5$ meV Å. We find the behavior to be qualitatively different in the two cases. In the latter case, $V_0 \to \infty$ as $E \to 0$ and the defect potential strength V_0 can change sign, which opens up the possibility of realizing subgap bound states for both potential wells and barriers of various sizes. Here, *1* and *2*, denoted by the solid and dashed curves, respectively, refer to the two solutions obtained for the strength of the potential V_0. The dashed line refers to the value of the energy gap, which is given by $2|\mu'|$ for the topologically trivial regime in (a) and $2E_g$ for the topologically nontrivial regime in (b). See discussion in main text for a comparison with the result in Ref. [41].

V_0 is always positive in this case, corresponding to holelike states near the valence band.

2. Inverted band gap: $\mu' < 0$

When the chemical potential intersects the lower surface conduction band, we have $\mu' < 0$. Evaluating the resulting integral from Eq. (15), we obtain the relation

$$V_{0,\pm} = \frac{4A(\sqrt{a}+\sqrt{b})}{[1-\sqrt{(1\pm\epsilon)/(1\mp\epsilon)}]}, \tag{29}$$

where $a, b = (|\mu'|/A)[\lambda - 1 \mp \sqrt{(\lambda-1)^2 - (1-\epsilon^2)}]$. Clearly, in this case, the amplitude of the defect potential may change sign depending on the value of the bound-state energy E under consideration, and in general, subgap bound states can be realized for both potential wells and barriers, corresponding to particle-like and holelike states, as is also evident from Fig. 5. The defect potential strength corresponding to the bound-state solutions move further away as we approach $\epsilon \to 0$, as illustrated in Fig. 5(b). In the limit $V_0 \to \infty$, we find a doubly degenerate zero-energy bound state, reminiscent of twofold degenerate zero-energy bound states in the honeycomb Kitaev model with a missing site [50,51]. Such a correspondence is perhaps unsurprising, given that the honeycomb Kitaev model sits on the verge of a transition to a chiral p-wave superconductor [52].

Similarly, for a finite, real value of k_y, we obtain the relation

$$V_{0,\pm} = \frac{2A(\sqrt{a}+\sqrt{b})\sqrt{1\mp\epsilon_e}(\sqrt{1\pm\epsilon_e}-\sqrt{1\mp\epsilon_e})}{\left(\sqrt{1-\epsilon_e^2}-1\right)},$$

where $\mu_e = \mu' - Ak_y^2$, $E_e^2 = E^2 - \Delta^2 k_y^2$, and $a, b = (|\mu_e|/A)[\lambda_e - 1 \mp \sqrt{(\lambda_e-1)^2-(1-\epsilon_e^2)}]$. Note that the above expression is only applicable in the regime where $\epsilon_e^2 < 1$.

On the other hand, for $\epsilon_e^2 > 1$, which can only be satisfied for $\mu' < 0$, we have the alternate expression

$$V_{0,\pm} = \frac{4A^2\sqrt{b}(b+a)[Ab+|\mu_e|(1\pm\epsilon_e)]}{\left[A^2b^2+2A|\mu_e|b+\mu_e^2(1-\epsilon_e^2)\right]}, \tag{30}$$

where $a, b = (\mu_e/A)[\sqrt{(\lambda_e-1)^2-(1-\epsilon_e^2)} \mp (\lambda_e - 1)]$. The right-hand side in Eq. (30) may change sign for bound-state energies satisfying the condition $|\epsilon_e| > \lambda_e$.

Apart from the above two kinds of isolated potential defects, one can also consider situations where the surface of the topological crystalline insulator is homogeneously disordered. In Appendix-A, we have determined the optimal potential fluctuation for realizing zero-energy bound states by adapting a Lifshitz-tail like treatment from the literature on disordered conductors. For homogeneously distributed one-dimensional defects (with translational symmetry preserved along one of the directions), we have confirmed that no zero-energy states can be realized in the topologically nontrivial situation where the chemical potential intersects the lower surface conduction band.

VI. CONCLUSIONS

In summary, we have examined the parameter regimes where a stable chiral p-wave superconducting order can exist on the (001) surface of $Pb_{1-x}Sn_xTe$, depending on the position of the chemical potential and the strength of the Zeeman splitting. Within the chiral p-wave regime, we further identified two situations, corresponding to the *normal* and the *inverted* band gap and showed that while Shiba-like states can exist in both these regimes, only in the latter case can the subgap states be attributed to the presence of a chiral p-wave superconducting order. By tuning the chemical potential in the latter regime, one can use local probes to identify the nature of the superconducting order observed on the (001) surface of $Pb_{1-x}Sn_xTe$. Shiba-like states could be a more reliable probe for detecting topological superconductivity in this material, as compared to the conventional strategy of detecting zero-bias anomalies, putatively Majorana bound states. This is particularly important since it has been shown in recent studies of $Pb_{1-x}Sn_xTe$ that even at high temperatures, when superconductivity is absent, zero-bias anomalies sharing many features that are traditionally attributed to Majorana bound states can appear, due to the presence of stacking faults [34,53]. The possibility of such errors arising in the interpretation of zero-bias anomalies have also been discussed in the context of other topological materials [33].

As a possible application of our results, we show that for the case of point defects, the wave functions corresponding to the zero-energy bound states have an internal SU(2) rotational symmetry, which makes them useful as possible quantum qubits. In an earlier work [41], the crossing of the particle-like and holelike impurity bound-state solutions at zero energy was identified as a signature for topological superconductivity, and we show that this is an artifact related to the BdG structure of the Hamiltonian and would occur even when applied to a nonsuperconducting system such as a semiconductor. The asymptotic behavior of the bound-state wave functions has also been calculated in the literature and found to be exponentially decaying [44]; however, this work assumes a constant density of states at the Fermi level, and this difference manifests itself in different decay lengths obtained for the exponential decay in the two cases. Interestingly, we found similarities between properties of the bound states realized on the surface of the TCI, and those associated with missing sites in the honeycomb Kitaev model [50,51,54,55], possibly arising from the fact that the latter sits on the verge of a chiral p-wave superconducting transition and can indeed be made to exhibit it on doping [52]. These similarities will be explored further in future work.

This analytical strategy could also be used to study bound states in defects with other symmetries. One interesting case to consider would be that of a semi-infinite line defect, modeled by a two-dimensional Delta-function potential $V(r,\phi) = \lambda\delta(\phi)$. The interesting thing here would be to look for the zero-energy Majorana bound state at $r = 0$ and obtain its wave function analytically. One can also study problems involving junctions of line defects or regular arrays of defects. Our approach can also be applied to other types of unconventional superconductivity, such as a chiral d-wave order.

ACKNOWLEDGMENTS

S.K. and V.T. thank Professor Kedar Damle for useful discussions. V.T. acknowledges DST for a Swarnajayanti grant (Grant No. DST/SJF/PSA-0212012-13).

APPENDIX A: OPTIMAL POTENTIAL FLUCTUATION FOR HOMOGENEOUSLY DISTRIBUTED DEFECTS

We consider homogeneously distributed one-dimensional defects on the surface of the TCI, such that translational symmetry is preserved along one of the directions. We first discuss the approach used for determining the optimal potential fluctuation in the case of a spatially uncorrelated potential disorder with a Gaussian distribution. We follow a statistical approach (see, for example, Ref. [56]), assuming that the disorder may be represented by a random potential $U(x)$ with a short-range Gaussian distribution, whose statistical properties are described by a probability measure $P[U]$, i.e.,

$$P[U] = \exp\left[-\frac{1}{2\gamma^2}\int d^dx d^dx'\, U(x)K^{-1}(x-x')U(x')\right], \tag{A1}$$

where the spatial correlation function for the disorder is given by $< U(x)U(x') >= \gamma^2 K(x-x') \equiv \gamma^2\delta(x-x')$.

In order to obtain the most probable potential distribution, at a fixed value for the bound-state energy E, we need to minimize the following functional over $U(x)$,

$$F[U(x), \psi(x)] = \int d\Omega\ U^2(x) - \eta \int d\Omega\ \psi^\dagger(x)(H-E)\psi(x),$$

where $H = A\sigma_3\nabla^2 - i\Delta\sigma_1\nabla - \mu'\sigma_3 + U(x)\sigma_3$ for a parabolic dispersion, which gives us the relation $U(x) = \frac{\eta}{2}\psi^\dagger(x)\sigma_3\psi(x)$. Using this condition to eliminate η, we now self-consistently solve the Schrödinger equation in the presence of chiral p-wave superconductivity on the surface and calculate the optimal potential distribution $U(x)$.

In the presence of a chiral p-wave superconducting order on the surface, the Schrödinger equation may be written as follows:

$$A\sigma_3\frac{d^2\psi}{dx^2} - i\Delta\sigma_1\frac{d\psi}{dx} - \mu'\sigma_3\psi + V_0(\psi^\dagger\sigma_3\psi)\sigma_3\psi = 0, \tag{A2}$$

where $V_0 = \eta/2$, and we specifically consider a zero-energy bound state, such that $k_y = 0$. The process of solving Eq. (A2) is enormously simplified by performing a gauge transformation, given by $\psi = \exp[iW(x-x_0)]\Phi$. Note that such a transformation becomes necessary only due to the presence of the chiral p-wave superconducting order. The same transformation works in the absence of p-wave superconductivity, with $W = 0$.

The matrix W may be chosen such that the coefficient of $d\Phi/dx$ vanishes, i.e., $2A\sigma_3(W) = \triangle\sigma_1$ and $W = [1/(2A)]\Delta i\sigma_2$. Substituting this back into Eq. (A2), we find

$$\begin{aligned} &A\sigma_3W^2\exp[iW(x-x_0)]\Phi + A\sigma_3\exp[iW(x-x_0)]\frac{d^2\Phi}{dx^2} - \mu'\sigma_3\exp[iW(x-x_0)]\Phi \\ &+ V_0(\Phi^\dagger\exp[-iW^\dagger(x-x_0)]\sigma_3\exp[iW(x-x_0)]\Phi)\sigma_3\exp[iW(x-x_0)]\Phi = 0. \end{aligned} \tag{A3}$$

The gauge-transformation leaves σ_3 invariant, i.e., $\exp[-iW^\dagger(x-x_0)]\sigma_3\exp[iW(x-x_0)] = \sigma_3$.

Multiplying Eq. (A3) by $\exp[-iW^\dagger(x-x_0)]$ throughout and replacing W^2 by $(-\Delta^2/(4A^2))I$, we arrive at the condition

$$-\frac{\Delta^2}{4A}\sigma_3\Phi + A\sigma_3\frac{d^2\Phi}{dx^2} - \mu'\sigma_3\Phi + V_0(\Phi^\dagger\sigma_3\Phi)\sigma_3\Phi = 0. \tag{A4}$$

The Hermitian conjugate of the above equation is given by

$$-\frac{\Delta^2}{4A}\Phi^\dagger\sigma_3 + A\frac{d^2\Phi^\dagger}{dx^2}\sigma_3 - \mu'\Phi^\dagger\sigma_3 + V_0(\Phi^\dagger\sigma_3\Phi^\dagger)\sigma_3\Phi = 0. \tag{A5}$$

We multiply Eq. (A4) on the left by $d\Phi^\dagger/dx$ and Eq. (A5) on the right by $d\Phi/dx$ and, adding the resulting set of equations, arrive at the expression

$$A\frac{d\Phi^\dagger}{dx}\sigma_3\frac{d\Phi}{dx} = \mu'\left(\mp\frac{\lambda}{2}+1\right)(\Phi^\dagger\sigma_3\Phi) - \frac{V_0}{2}(\Phi^\dagger\sigma_3\Phi)^2, \tag{A6}$$

where λ is as defined in Eq. (5) and the signs $\mp$ correspond to $\mu' < 0$ and $\mu' > 0$, respectively. For simplicity, let us consider a solution of the form $\Phi = \binom{a}{b}$, where $a(x)$ and $b(x)$ are assumed to be real functions. Then, Eq. (A6) gives us the condition

$$A\left[\left(\frac{da}{dx}\right)^2 - \left(\frac{db}{dx}\right)^2\right] = \mu'\left(\frac{\mp\lambda}{2}+1\right)(a^2-b^2) - \frac{V_0}{2}(a^2-b^2)^2.$$

We find that one may obtain solutions for the special cases where $a = 0$ or $b = 0$, i.e., $\Phi = \binom{a}{0}$ or $\Phi = \binom{0}{b}$. This leads to the following set of equations:

$$A\left(\frac{da}{dx}\right)^2 = \mu'\left(\mp\frac{\lambda}{2} + 1\right)a^2 - \frac{V_0}{2}a^4, \tag{A7}$$

$$A\left(\frac{db}{dx}\right)^2 = \mu'\left(\mp\frac{\lambda}{2} + 1\right)b^2 + \frac{V_0}{2}b^4. \tag{A8}$$

It can be seen from Eqs. (A7) and (A8) that in the topologically nontrivial regime with $\mu' < 0$, where $\lambda \leqslant 2$, the above equations cannot give rise to zero-energy bound-state solutions for any value of V_0.

Now, simplifying Eq. (A7), we have

$$\frac{1}{\sqrt{C_1}}\frac{da}{dx} = \xi\frac{a}{\sqrt{C_1}}\sqrt{1 - \frac{a^2}{C_1}},$$

where $C_1 = 2\mu'[\mp(\lambda/2) + 1]/V_0$. This can be rewritten as

$$\frac{d\alpha}{\alpha\sqrt{1-\alpha^2}} = \xi dx,$$

where $\alpha(x) = a(x)/\sqrt{C_1}$ and $\xi = \sqrt{V_0/(2A)}\sqrt{C_1} = \sqrt{(\mu'/A)[\mp(\lambda/2) + 1]}$. Integrating both sides, we find

$$\text{ArcSech}[\alpha_0] - \text{ArcSech}[\alpha(x)] = \xi(x - x_0),$$

where $\alpha_0 = \alpha(x_0)$. Let us define $\Lambda_0 = \text{ArcSech}[\alpha_0]$. Then the solution for $a(x)$ is given by

$$a(x) = \frac{\sqrt{C_1}}{\cosh[\Lambda_0 - \xi(x - x_0)]}. \tag{A9}$$

A similar procedure can be followed for Eq. (A8) above, provided $V_0 < 0$.

APPENDIX B: DERIVATION OF THE ASYMPTOTIC FORM OF THE BOUND-STATE WAVE FUNCTIONS FOR POINT DEFECTS

Here we derive the expressions for the asymptotic form of the bound-state wave functions in the case of a point defect.

The expression for the bound-state wave functions for point defects involves the following integrals:

$$I_1(r) = -\frac{1}{(2\pi)^2}\int kdkd\phi\exp\{ikr\cos[\theta - \phi]\}\frac{(Ak^2 + \mu')}{(Ak^2 + \mu')^2 + \Delta^2k^2}$$

and

$$I_2(r,\theta) = \frac{1}{(2\pi)^2}\int kdkd\phi\exp\{ikr\cos[\theta - \phi]\}\exp[i\phi]\frac{\Delta k}{(Ak^2 + \mu')^2 + \Delta^2k^2},$$

where $k = \sqrt{k_x^2 + k_y^2}$, $\tan[\phi] = \frac{y}{x}$. Let us now consider the integral I_1. Using the result $\int d\phi\exp\{ikr\cos[\theta - \phi]\} = 2\pi J_0(kr)$, we have

$$I_1(r) = -\frac{1}{(2\pi)^2}\int kdk\frac{Ak^2 + \mu'}{(Ak^2 + \mu')^2 + \Delta^2k^2}2\pi J_0(kr).$$

The above expression may be rewritten as

$$\begin{aligned} I_1 &= -\frac{1}{2\pi}\int kdk\frac{\frac{1}{2}(Ak^2 + \mu' + i\Delta k) + \frac{1}{2}(Ak^2 + \mu' - i\Delta k)}{(Ak^2 + \mu')^2 + \Delta^2k^2}J_0(kr) \\ &= -\frac{1}{4\pi}\int dkkJ_0(kr)\frac{1}{A}\left[\frac{1}{(k - k_1)(k - k_2)} + \frac{1}{(k - k_3)(k - k_4)}\right], \end{aligned}$$

where $k_1 = i\sqrt{\frac{\mu'}{A}}\frac{\sqrt{\lambda+2}+\sqrt{\lambda}}{\sqrt{2}}$, $k_2 = i\sqrt{\frac{\mu'}{A}}\frac{\sqrt{\lambda}-\sqrt{\lambda+2}}{\sqrt{2}}$, $k_3 = i\sqrt{\frac{\mu'}{A}}\frac{\sqrt{\lambda+2}-\sqrt{\lambda}}{\sqrt{2}} = -k_2$, $k_4 = -i\sqrt{\frac{\mu'}{A}}\frac{\sqrt{\lambda+2}+\sqrt{\lambda}}{\sqrt{2}} = -k_1$. This can further be simplified as

$$-\frac{1}{4\pi}\int dkkJ_0(kr)\frac{1}{A(k_1 - k_2)}\left(\frac{2k_1}{k^2 - k_1^2} - \frac{2k_2}{k^2 - k_2^2}\right).$$

Let us now rewrite $k_1 = i\alpha, k_2 = -i\beta$, where α and β are real, and $\alpha, \beta > 0$ ($\alpha = \sqrt{\frac{\mu'}{A}}\frac{\sqrt{\lambda+2}+\sqrt{\lambda}}{\sqrt{2}}$, $\beta = \sqrt{\frac{\mu'}{A}}\frac{\sqrt{\lambda+2}-\sqrt{\lambda}}{\sqrt{2}}$). The above equation can be rewritten as

$$-\frac{1}{4\pi}\int dk k J_0(kr)\frac{2}{A(\alpha+\beta)}\left(\frac{\alpha}{k^2+\alpha^2}+\frac{\beta}{k^2+\beta^2}\right).$$

To evaluate the above expression, we shall use the standard integral [49].

$$\int_0^\infty dk\frac{kJ_0(kr)}{k^2+\alpha^2} = K_0(\alpha r),$$

which is applicable in our case, since $r > 0$, α, β are real and $\mathrm{Re}[\alpha], \mathrm{Re}[\beta] > 0$. The asymptotic form of the right-hand side is given by

$$K_0(\alpha r) \sim \left(\frac{\pi}{2\alpha r}\right)^{1/2}\exp[-\alpha r]\sum_{n=0}^{\infty}\frac{a_n(0)}{(\alpha r)^n},$$

where $a_n(\nu) = \frac{(4\nu^2-1^2)(4\nu^2-3^2)\ldots[4\nu^2-(2n+1)^2]}{(n+1)!}[\frac{1}{4\nu^2-1^2}+\frac{1}{4\nu^2-2^2}+\ldots\frac{1}{4\nu^2-(2n+1)^2}]$. Using these results, we find

$$I_1(r) = -\frac{1}{2\pi A(\alpha+\beta)}[\alpha K_0(\alpha r)+\beta K_0(\beta r)],$$

which is an exponentially decaying function at large values of r.

Similarly, using the result $\int d\phi \exp\{ikr\cos[\theta-\phi]\}\exp[i\phi] = i2\pi J_1(kr)\exp[i\theta]$, we may simplify the expression for I_2 as

$$\begin{aligned}
I_2(r,\theta) &= \frac{\exp[i\theta]}{(2\pi)^2}\int kdk\frac{\Delta k}{(Ak^2+\mu')^2+\Delta^2k^2}i2\pi J_1(kr)\\
&= \frac{\exp[i\theta]}{2\pi}\int dkkJ_1(kr)\frac{1}{2}\left(\frac{1}{Ak^2+\mu'-i\Delta k}-\frac{1}{Ak^2+\mu'+i\Delta k}\right)\\
&= \frac{\exp[i\theta]}{4\pi}\int dkkJ_1(kr)\frac{1}{A(k_1-k_2)}\left(\frac{1}{k-k_1}-\frac{1}{k-k_2}+\frac{1}{k+k_1}-\frac{1}{k+k_2}\right)
\end{aligned}$$

$k_1 = i\sqrt{\frac{\mu'}{A}}\frac{\sqrt{\lambda+2}+\sqrt{\lambda}}{\sqrt{2}}$, $k_2 = i\sqrt{\frac{\mu'}{A}}\frac{\sqrt{\lambda}-\sqrt{\lambda+2}}{\sqrt{2}}$, $k_3 = i\sqrt{\frac{\mu'}{A}}\frac{\sqrt{\lambda+2}-\sqrt{\lambda}}{\sqrt{2}} = -k_2$, $k_4 = -i\sqrt{\frac{\mu'}{A}}\frac{\sqrt{\lambda+2}+\sqrt{\lambda}}{\sqrt{2}} = -k_1$. This can be rewritten as

$$\frac{\exp[i\theta]}{4\pi}\int dkkJ_1(kr)\frac{1}{A(k_1-k_2)}\left(\frac{2k}{k^2-k_1^2}-\frac{2k}{k^2-k_2^2}\right).$$

Again, replacing k_1 by $i\alpha$ and k_2 by $-i\beta$, where α and β are real, and $\alpha, \beta > 0$ ($\alpha = \sqrt{\frac{\mu'}{A}}\frac{\sqrt{\lambda+2}+\sqrt{\lambda}}{\sqrt{2}}$, $\beta = \sqrt{\frac{\mu'}{A}}\frac{\sqrt{\lambda+2}-\sqrt{\lambda}}{\sqrt{2}}$), we find

$$I_2 = \frac{\exp[i\theta]}{4\pi}\int dkJ_1(kr)\frac{2}{Ai(\alpha+\beta)}\left(\frac{k^2}{k^2+\alpha^2}-\frac{k^2}{k^2+\beta^2}\right).$$

Let us rewrite the variable of integration as $kr \equiv x$. Then

$$I_2 = \frac{\exp[i\theta]}{2\pi Ai(\alpha+\beta)}\int\frac{dx}{r}J_1(x)\left(\frac{x^2}{x^2+\alpha^2r^2}-\frac{x^2}{x^2+\beta^2r^2}\right). \tag{B1}$$

To evaluate the above Eq. (B1), we shall use the standard integral [49],

$$\int_0^\infty dx\frac{xJ_0(ax)}{x^2+\alpha^2r^2} = K_0(a\alpha r),$$

where $r > 0$, α, β are real and $\mathrm{Re}[\alpha], \mathrm{Re}[\beta] > 0$. Here we differentiate both sides with respect to a and then take the limit $a \to 1$, we have

$$\int_0^\infty\frac{x^2J_1(x)}{x^2+\alpha^2r^2}dx = K_1(\alpha r). \tag{B2}$$

Thus, using Eq. (B2) in Eq. (B1), we have

$$I_2 = \frac{\exp[i\theta]}{2\pi Ai(\alpha+\beta)r}[K_1(\alpha r) - K_1(\beta r)].$$

The asymptotic form of the function on the right-hand side is given by

$$K_1(\alpha r) \sim \left(\frac{\pi}{2\alpha r}\right)^{1/2} \exp[-\alpha r] \sum_{n=0}^{\infty} \frac{a_n(1)}{(\alpha r)^n}.$$

where $a_n(\nu) = \frac{(4\nu^2-1^2)(4\nu^2-3^2)...[4\nu^2-(2n+1)^2]}{(n+1)!}[\frac{1}{4\nu^2-1^2} + \frac{1}{4\nu^2-2^2} + \cdots \frac{1}{4\nu^2-(2n+1)^2}]$, which is exponentially decaying in nature.

[1] M. Leijnse and K. Flensberg, Semicond. Sci. Technol. **27**, 124003 (2012).
[2] J. Alicea, Rep. Prog. Phys. **75**, 076501 (2012).
[3] M. Sato and Y. Ando, Rep. Prog. Phys. **80**, 076501 (2017).
[4] Q. L. He, L. Pan, A. L. Stern, E. C. Burks, X. Che, G. Yin, J. Wang, B. Lian, Q. Zhou, E. S. Choi, K. Murata, X. Kou, Z. Chen, T. Nie, Q. Shao, Y. Fan, S.-C. Zhang, K. Liu, J. Xia, and K. L. Wang, Science **357**, 294 (2017).
[5] R. M. Lutchyn, E. P. A. M. Bakkers, L. P. Kouwenhoven, P. Krogstrup, C. M. Marcus, and Y. Oreg, Nat. Rev. Mater. **3**, 52 (2018).
[6] L. Fu and C. L. Kane, Phys. Rev. Lett. **100**, 096407 (2008).
[7] J. D. Sau, R. M. Lutchyn, S. Tewari, and S. Das Sarma, Phys. Rev. Lett. **104**, 040502 (2010).
[8] R. M. Lutchyn, J. D. Sau, and S. Das Sarma, Phys. Rev. Lett. **105**, 077001 (2010).
[9] A. Y. Kitaev, Phys.- Usp. **44**, 131 (2001).
[10] R. Aguado, La Rivista del Nuovo Cimento **40**, 523 (2017).
[11] C. Kallin and A. J. Berlinsky, J. Phys.: Condens. Matter **21**, 164210 (2009).
[12] Y. Maeno, S. Kittaka, T. Nomura, S. Yonezawa, and K. Ishida, J. Phys. Soc. Jpn. **81**, 011009 (2012).
[13] C. Kallin, Rep. Prog. Phys. **75**, 042501 (2012).
[14] S. Sasaki, M. Kriener, K. Segawa, K. Yada, Y. Tanaka, M. Sato, and Y. Ando, Phys. Rev. Lett. **107**, 217001 (2011).
[15] Y. Ando, K. Segawa, S. Sasaki, and M. Kriener, J. Phys.: Conf. Ser. **449**, 012033 (2013).
[16] M. Kriener, K. Segawa, Z. Ren, S. Sasaki, and Y. Ando, Phys. Rev. Lett. **106**, 127004 (2011).
[17] Superconductivity does not exist in the bulk as the bulk bands are completely occupied in the topological insulator state.
[18] S. Kundu and V. Tripathi, Phys. Rev. B **96**, 205111 (2017).
[19] S. Kundu and V. Tripathi, Eur. Phys. J. B **91**, 198 (2018).
[20] N. Furukawa, T. M. Rice, and M. Salmhofer, Phys. Rev. Lett. **81**, 3195 (1998).
[21] Y. Tanaka, T. Shoman, K. Nakayama, S. Souma, T. Sato, T. Takahashi, M. Novak, K. Segawa, and Y. Ando, Phys. Rev. B **88**, 235126 (2013).
[22] Y. Tanaka, Z. Ren, T. Sato, K. Nakayama, S. Souma, T. Takahashi, K. Segawa, and Y. Ando, Nat. Phys. **8**, 800 (2012).
[23] T. H. Hsieh, H. Lin, J. Liu, W. Duan, A. Bansil, and L. Fu, Nat. Commun. **3**, 982 (2012).
[24] J. Liu, W. Duan, and L. Fu, Phys. Rev. B **88**, 241303(R) (2013).
[25] S.-Y. Xu, C. Liu, N. Alidoust, M. Neupane, D. Qian, I. Belopolski, J. Denlinger, Y. Wang, H. Lin, L. Wray *et al.*, Nat. Commun. **3**, 1192 (2012).
[26] P. Dziawa, B. Kowalski, K. Dybko, R. Buczko, A. Szczerbakow, M. Szot, E. Łusakowska, T. Balasubramanian, B. M. Wojek, M. Berntsen *et al.*, Nat. Mater. **11**, 1023 (2012).
[27] Y. J. Wang, W.-F. Tsai, H. Lin, S.-Y. Xu, M. Neupane, M. Z. Hasan, and A. Bansil, Phys. Rev. B **87**, 235317 (2013).
[28] H. Yao and F. Yang, Phys. Rev. B **92**, 035132 (2015).
[29] I. Dzyaloshinskii, JETP Lett. **46**, 118 (1987).
[30] S. Das, L. Aggarwal, S. Roychowdhury, M. Aslam, S. Gayen, K. Biswas, and G. Sheet, Appl. Phys. Lett. **109**, 132601 (2016).
[31] G. Mazur, K. Dybko, A. Szczerbakow, M. Zgirski, E. Lusakowska, S. Kret, J. Korczak, T. Story, M. Sawicki, and T. Dietl, arXiv:1709.04000.
[32] G. Sheet, S. Mukhopadhyay, and P. Raychaudhuri, Phys. Rev. B **69**, 134507 (2004).
[33] Y.-C. Yam, S. Fang, P. Chen, Y. He, A. Soumyanarayanan, M. Hamidian, D. Gardner, Y. Lee, M. Franz, B. I. Halperian, E. Kaxiras, and J. E. Hoffman, arXiv:1810.13390.
[34] P. Sessi, D. Di Sante, A. Szczerbakow, F. Glott, S. Wilfert, H. Schmidt, T. Bathon, P. Dziawa, M. Greiter, T. Neupert, G. Sangiovanni, T. Story, R. Thomale, and M. Bode, Science **354**, 1269 (2016).
[35] M. Wimmer, A. R. Akhmerov, M. V. Medvedyeva, J. Tworzydlo, and C. W. J. Beenakker, Phys. Rev. Lett. **105**, 046803 (2010).
[36] Y. Luh, Acta Phys. Sin. **21**, 75 (1965).
[37] H. Shiba, Prog. Theor. Phys. **40**, 435 (1968).
[38] A. Rusinov, JETP Lett. (USSR) **9**, 146-9 (1969).
[39] K. Maki and S. Haas, Phys. Rev. B **62**, R11969 (2000).
[40] Q.-H. Wang and Z. D. Wang, Phys. Rev. B **69**, 092502 (2004).
[41] J. D. Sau and E. Demler, Phys. Rev. B **88**, 205402 (2013).
[42] M. Mashkoori, K. Bjornson, and A. M. Black-Schaffer, Sci. Rep. **7**, 44107 (2017).
[43] F. Wang, Q. Liu, T. Ma, and X. Jiang, J. Phys.: Condens. Matter **24**, 455701 (2012).
[44] V. Kaladzhyan, C. Bena, and P. Simon, J. Phys.: Condens. Matter **28**, 485701 (2016).
[45] V. Kaladzhyan, J. Röntynen, P. Simon, and T. Ojanen, Phys. Rev. B **94**, 060505(R) (2016).
[46] V. Kaladzhyan, C. Bena, and P. Simon, Phys. Rev. B **93**, 214514 (2016).
[47] S. Haas and K. Maki, Phys. Rev. Lett. **85**, 2172 (2000).
[48] In contrast, in long linear defects, these impurity bound states form a band, which makes it harder to isolate the qubit from the environment. The two qubits are, however, of different types, and the latter is specifically relevant for topological quantum computation.

[49] I. S. Gradshteyn and I. M. Ryzhik, *Table of Integrals, Series, and Products*, 7th ed. (Elsevier/Academic Press, Amsterdam, 2007).

[50] A. J. Willans, J. T. Chalker, and R. Moessner, Phys. Rev. B **84**, 115146 (2011).

[51] A. J. Willans, J. T. Chalker, and R. Moessner, Phys. Rev. Lett. **104**, 237203 (2010).

[52] Y.-Z. You, I. Kimchi, and A. Vishwanath, Phys. Rev. B **86**, 085145 (2012).

[53] D. Iaia, C.-Y. Wang, Y. Maximenko, D. Walkup, R. Sankar, F. Chou, Y.-M. Lu, and V. Madhavan, Phys. Rev. B **99**, 155116 (2019).

[54] K. Dhochak, R. Shankar, and V. Tripathi, Phys. Rev. Lett. **105**, 117201 (2010).

[55] S. D. Das, K. Dhochak, and V. Tripathi, Phys. Rev. B **94**, 024411 (2016).

[56] A. Altland and B. D. Simons, *Condensed Matter Field Theory*, 2nd ed. (Cambridge University Press, Cambridge, 2010).